

The Future of the South Atlantic Anomaly And Implications for Radiation Damage in Space

J. R. Heirtzler*

*Laboratory for Terrestrial Physics, NASA/Goddard Space Flight Center
Greenbelt, MD 20771*

Abstract

The South Atlantic Anomaly of the geomagnetic field plays a dominant role in where radiation damage occurs in near Earth orbits. The historic and recent variations of the geomagnetic field in the South Atlantic are used to estimate the extent of the South Atlantic Anomaly until the year 2000. This projection indicates that radiation damage to spacecraft and humans in space will greatly increase and cover a much larger geographic area than present.

1. Introduction

In order to understand what might be the future radiation hazard of the South Atlantic Anomaly it will be necessary to briefly review how the geomagnetic field is related to the radiation hazard in Low Earth Orbit at the present time. It has been known for more than 40 years that there is a weak geomagnetic field in the South Atlantic Ocean, known as the South Atlantic Anomaly (SAA). This coincides with a region of intense radiation in space near the Earth. This intense radiation causes damage to the many spacecraft in Low Earth Orbit and is a hazard to astronauts/cosmonauts which are there. The basic physical laws governing charged particle motion in the geomagnetic field are well understood, although significant questions remain about the density of charged particles with respect to their energy and how this varies with time.

Of the three well known types of charged particle motion in the

*Fax: 301-614-6015

Email: jamesh@ltpmail.gsfc.nasa.gov

geomagnetic field (gyrorotation about the geomagnetic line of force, the bounce of the particles from hemisphere to hemisphere, with mirror points in each hemisphere and the drift of particles to the east or west because of the longitudinal variation of field strength) only the bounce motion will be considered here. It is the lower mirror points over the SAA that is generally thought responsible for the more intense radiation there, because, there is more interaction with the atmosphere there. We will examine this point, looking at the configuration of the geomagnetic field and the places where radiation damage occurs. The reader is referred to other publications for discussions of the various models of radiation in space (e.g. Lemaire and others, 1996). Here we will only illustrate how the radiation associated with the geomagnetic field to better understand the role of the SAA.

awkward

? something is missing.

2. Configuration of the Geomagnetic Field

We need only consider the total intensity of the field rather than its directional components, although for ray tracing one needs to use the declination and inclination of the geomagnetic field vector. As usual we use a spherical harmonic expression of the geomagnetic potential, with coefficients and their time derivatives for 1995, as given by Barton, C.E., et al. (1996 This International Geomagnetic Reference Field (IGRF 95) was used as an input to a computer subroutine to give the components and total field at any latitude, longitude, altitude, and time. This data was used to graphically display various aspects of the field.

Figure 1 is a contour plot of the total field for the year 1995.0 at the Earth's surface. It shows the SAA, which has a minimum value of about 23,000 nT located about 700 km inland from the coast of Southern Brazil. Also shown are the highs in the Canadian Arctic, Siberia, and in Antarctic south of Australia. The SAA is generally said to be due to the fact that the inclined dipole axis of the Earth is displaced in the direction of the northwest Pacific (21.47 N, 144.77 E) by 527 km (Frazier-Smith, 1987). In fact when the geomagnetic field of the Earth is plotted using only the inclined, offset axis terms, the low in the South Atlantic is somewhat differently shaped from the SAA shown in Figure 1, indicating that the SAA has a contribution from the higher order terms of the IGRF.

Contrary to common approximations, the geomagnetic field near the Earth differs significantly from a dipole. Contour plots of the total field were

made at altitudes of 200 km, 500 km, 1000 km, and 5000 km. It is only at 5000 km (0.78 Earth radii) that the contours of field strength resemble those of the inclined offset dipole. At 10,000 km the field strength is reduced to about one-tenth its surface value. At 15,000 km (2.35 Earth radii) the field resembles that of an inclined axial dipole.

Since the SAA is determined by the configuration of the geomagnetic field lines, a ray tracing program, using the IGRF 95, was written and used to plot the geomagnetic field lines (details of this program are given in Heirtzler, 1999). As an illustration of the asymmetry of the geomagnetic field lines on different sides of the Earth, Figure 2 shows field lines which originate along the longitudes 40 W and 140 E at latitudes 20 S, 40 S, and 60 S. Note that 40W is near the longitude of the SAA and 140 E is near the longitude of the Siberian and Antarctic highs. Notice that the line which leaves 60 S terminates near 80 N along 140 E, but at about 40 N along 40 W. As the Earth rotates during the course of a day this asymmetry with respect to the rotational axis creates a changing, magnetically complex region in near space.

The ray tracing program which generated field values along a line of force was used to locate the magnetic equator, where the dip angle changed sign, in order to determine the value of the equatorial field value there. Knowing this field value (B_e) one can calculate the field value for the mirror point (B_m) for any equatorial pitch angle (θ_e) by the relationship

$$B_e / \sin^2(\theta_e) = B_m / \sin^2(\theta_m) = B_m \quad \text{Eq.(1)}$$

since at the mirror point the pitch angle $\theta_m = 90$ degrees. Using this value of B_m we can search along the line of force to find the position of the mirror point.

Figure 3 displays three lines of force starting at latitudes 40 S, 30 S, and 20 S, all along longitude 60 W. Points and numbers along each field line show the mirror points for different equatorial pitch angles. Actually particles do not reach altitudes lower than about 100 km because they are scattered or absorbed by the atmosphere there. The line which originates at 20 S is almost totally within the atmosphere and has few particles associated with it for the same reason.

A consideration of the line which starts at 40 S illustrates that particles with equatorial pitch angles of less than about 45 degrees (loss cone 45 degrees)

are removed from the *southern* end of the line, invalidating mirror points of less than this pitch angle on the *northern* end of the line. This same asymmetry is true on the other lines because of the low value of the SAA.

In considering how these mirror points might be related to the intensity of radiation in space one should be aware of how the number density of particles varies as a function of equatorial pitch angle. This is characterized by the anisotropy index n in the equation for the distribution function $J(\alpha)$ ← ?

$$J(\alpha) = J \sin^n(\alpha) \quad \leftarrow \text{Eq. (2)} \quad ?$$

Where J is the value of $J(\alpha)$ when $\alpha = 90$ degrees. ?

Fung (1996) has shown that, for electrons and protons, n has values of 1 to 10, with the larger values more common. The relative probability $J(\alpha)/J$ is large, especially for larger values of n . This shows that most particles have high equatorial pitch angles, nearing 90 degrees. Thus most particles will be mirroring near the top of their field line trajectory, and relatively fewer particles will reach the atmosphere. For more explicit models of the radiation, with actual number density, rather than just anisotropy, the National Space Science Data Center has developed models AE-8 and AP-8 for electrons and protons, respectively. There are separate models for sunspot maximum and for sunspot minimum. ?

3. Damage in Low Earth Orbit

It is convenient to first look at the damage to spacecraft instruments and then to comment on the radiation hazard to humans. Although it is difficult to characterize any space mission as typical it is instructive to briefly consider well-documented cases of each of these two types of damage. The two types of damage are characterized by different types of particle and energy dependency.

Spacecraft suffer from several types of damage while in orbit.. These range from space debris, problems with the vacuum of space, various problems associated with the plasma environment, and various problems explicitly associated with the radiation environment. The radiation environment causes several types of hazards, but here we will look at one of the most common. This is the Sudden Event Upset (SEU), where, apparently, a single particle causes a

piece of equipment to malfunction. Most ground controllers keep records of SEU's and these records are archived at the National Geophysical Data Center in Boulder.

An example of where SEU's occurred for the Topex/Poseidon spacecraft is given in Figure 4, for the period 1992-1998. This spacecraft operated at an altitude of 1340 km, and the total geomagnetic field contours for this altitude are shown on the figure. As is characteristic, all the places where the SEU occurred do not precisely fall within any single contour line. (There is an even closer relationship between the SEU's and the McIlwain L-parameter. Here we use the geomagnetic field contour as a simple surrogate for the L-parameter.) In this case most SEU's occurred where the geomagnetic field was less than about 24,000 nT at this altitude. α

Magnetograms from geomagnetic observatories near the individual SEU's were examined for the time when these SEU occurred but these magnetograms showed no unusual behavior. The planetary Ap index was studied to see if this index was large at the times of the SEU's, indicating disturbed conditions. Again the Ap's for those times did not differ significantly in their statistical distribution from the Ap's for all time during 1992-1998. These observations show SEU's bear little relation to general disturbed conditions and must be accounted for by an individual charged particle. There were 282 SEU's in or near the SAA over this 6 year period. The record shows that there were a few per week to a few per month, depending upon the solar cycle, and this frequency seem characteristic of spacecraft with radiation hardened components.

One of the clearest illustrations of how the radiation dose rate for humans is related to the SAA is given in paper by Badhwar (1997) and shown here in Figure 5. The dose rate determined by dosimeter on board Skylab during December 1973 to January 1974 and Mir during March 2-11, 1995, are shown as functions of latitude and longitude. While this paper was written to show the change in location of the SAA over the 21.2 year period between the two data sets, it clearly defines the location of highest radiation dosages at the 400 km altitude of these two spacecraft. Mir's data shows that the peak in the dose curve extended from 10 S to 40 S and 5 W to 65 W in March of 1995. This approximately defines the 24,000 nT contour at 400 km altitude. However there are lesser, broader peaks in the Mir dose rates away from the SAA. α

These considerations show that the 24,000 nT contour may be used as a general guide, for the aeral extent of radiation damage to spacecraft or radiation hazards to humans for altitudes up to 1400 km.

4. The Future of the South Atlantic Anomaly

Precise predictions of the geomagnetic field, on almost any time scale, are well known to be impossible. However one can speak about average changes with a high probability of being correct. We will look at the historical record of past geomagnetic field changes and try to use that as a guide for estimating the most probable future field. Although measurements of magnetic inclination and declination extend back several centuries, the measurement of the geomagnetic intensity has only been possible since the time of Gauss, in 1833. Even at that time there were not enough measurements to draw accurate maps. One of the earliest world maps of the intensity was that for the year 1922 (Chapman and Bartels, 1940, p. 101) from records of the British Admiralty. If the map of secular change from the IGRF 95 coefficients (Figure 6) is used to extrapolate back from 1995 to 1922 the charts compare favorably in the South Atlantic. Sabaka, et al. (1997) have calculated secular variation for several epochs starting in the early parts of this century and, again, rates are similar to that of Figure 6.

In the literature several papers have reported changes in the center of the SAA with time (Pinto and Gonzalez , 1989; Golightly et al., 1994; Konradi et al., 1994; Lauriente et al., 1995; Badhwar et al., 1996; Badhwar, 1997). The more recent of these, which include larger data bases indicate an annual change of about 0.28 degrees W, 0.08 degrees N. If one uses the secular change coefficients in the IGRF 95 model, one obtains about the same values (0.20 degrees W, 0.02 degrees N per year) for the years 1973 - 1995. Since not all parts of the Earth have the same secular change the movement of the center of the SAA may be slightly different from that of the 24,000 nT contour. Also, as Heyndrickx (1996) has pointed out, one may define the center of the SAA in three ways: (a) the mirror point using the eccentric dipole approximation, (b) using the minimum of the geomagnetic field, as above, or (c) the locus of the particle flux maximum. These may differ from one another by 10 degrees of latitude and 20 degrees of longitude.

Figure 6 shows that the greatest rate of secular change of the intensity, at present, is in the South Atlantic, southwest of Cape Town, where the rate is more

than -100 nT/yr. There is a secondary area of rapid change of field strength in the North Atlantic where it exceeds -80 nT/yr. The IGRF 95 database carries a warning that it should not be extrapolated for more than a few years in the future if it is to be very accurate. This warning is justified because older historical data shows that the secular variation of directions of the field has been quite nonlinear in the past, for certain geomagnetic observatories, especially those in London, Hawaii, and in India but not for those around the South Atlantic. Here we are making the most reasonable estimate of the future field by multiplying the changes shown in Figure 6 by the number of years of change and adding that to the 1995 field shown in Figure 1.

✓ The process of making spherical harmonic models with a finite number of coefficients, such as the IGRF, necessitates smoothing over some values observed in making the model. Thus, if one wants to consider the future of the SAA, one should look carefully at the historical values which have been measured at geomagnetic observatories around the South Atlantic. The National Geophysical Data Center has records from 25 observatories around the South Atlantic, with 11 of them having annual mean records of 25 years or more. These 11 show rates of change similar to those shown in Figure 6, except that Hermanus, South Africa, and Syowa Base, Antarctica, show somewhat greater change.

Figure 7 shows annual means from five observatories with longer records. The dashed line with each record is a least square fit to the data and the slope of this line is indicated. The location of these observatories is shown in the upper left panel. All stations show a nearly linear decrease with time and all, excepting, as mentioned before, Hermanus (HER), show values like that shown by the IGRF 95 secular change (see upper left panel). *Monthly* mean values for 3 of these observatories are available from Institute Physique Globe, Paris. Although the scatter of values is greater for the monthly means than for the annual means, a least squares fit to the monthly mean values yields values, as expected, very similar to those of the annual means.

The geological record of the paleomagnetic field provides little insight to changes in field strength on a time scale as short as 100 years. Creer et al. (1983) reported a paleomagnetic study of sediments from 3 lakes about 600 km northwest of the Trelew (TRW) observatory. The resolution of these measurements was not sufficient to yield information about the last few hundred years.

Using the IGRF 95 coefficients and their secular change the field was calculated and plotted for a number of years in the future. As an example Figure 8 is the field for the year 2100. It differs in several interesting and significant ways from the field for 1995 (Figure 1). The SAA, as defined by the 24,000 nT contour, covers a larger area of the South America, South Africa, and the South Atlantic. The SAA low has broken into two lows: one northwest of the present low of the SAA, and the other one southwest of Cape Town. In addition the low southwest of Cape Town is lower than the low of 1995. The map for 2100 shows relatively little change for the highs south of Australia, in Siberia and in northern Canada.

Figure 9 illustrates field lines for the year 2100 along the Greenwich Meridian (0 degrees longitude), with mirror points for particles with various equatorial pitch angles (contrast with Figure 3). The Greenwich Meridian was chosen for this illustration because that is where the low southwest of Cape Town is located in 2100 (Figure 7). When this figure is compared to Figure 3 it is seen that the particles with smaller equatorial pitch angles can reach the top of the atmosphere in the region of this new low for the SAA where they could not in Figure 3.

5. Conclusions

If the geomagnetic secular variation continues for the next hundred years, as it has for the past hundred years, the South Atlantic Anomaly can be expected to greatly increase. There will likely be a smooth increase in the shape of the SAA, from year to year, from its present size to the shape indicated for the year 2100. Intermediate values for the years 2025 and 2050 are shown in Heirtzler (1999). The present focus of the SAA will move northwest and a new and deeper focus will appear southwest of Africa, near the Greenwich Meridian and 50 degrees south. Numerous manned and unmanned spacecraft will be orbiting through this area.

The consequence of this change for radiation damage in space will be to make the radiation damage more intense and for it to cover an area several times as large as present. More particles will be absorbed in the atmosphere and this could alter the overall number of particles in the radiation belts. Furthermore, since the longitudinal distribution of the field affects the ring current, that, too, may be altered and have a more global effect. A calculation of the change in the

How many?
It is totally
invalid to project
the field this far
in the future.

dip equator with time shows that by the year 2100 it will have moved north by 10 to 15 degrees in the North Atlantic, but will have little changed elsewhere.

The large change expected in the future geomagnetic field indicates that more exact calculations should be made of the geographical extent and intensity of this damaging radiation for the safety of future near Earth missions. To better quantify these effects geomagnetic field measurements by satellites are important to keep track of the secular variation.

The year 2100 was used here to illustrate the change in the SAA with time but this change can be extrapolated to even longer times. Using this extrapolation, the low in the field strength southwest of Cape Town will be reduced to zero in the year 2240, and the SAA would cover about half of the southern hemisphere at that time. All components of the field will be zero.

Acknowledgements

The author acknowledges the support of NASA Goddard Space Flight Center and helpful comments by reviewers, although the views expressed are his own.

References

- Badhwar, Gautam D. 1997. Drift rate of the South Atlantic Anomaly, *Jour. Geophys. Res.*, 102, 2343-2349.
- Badhwar, G. D., et al. 1996. In flight radiation measurements on STS-60, *Radiat. Meas.*, 26, 17-34.
- Barton, C. E., and members of Working Group 8 1996. International geomagnetic reference field, 1995 revision, International Association of Geomagnetism and Aeronomy (IAGA) Division V, Working Group 8, *Geophys. J. Int.*, 125, 318-321.
- Creer, K. M., D. A. Valencio, A. M. Sinito, P. Tucholka and J. F. A. Vilas 1983. Geomagnetic secular variations 0-14000 yr BP as recorded by lake sediments from Argentina, *Geophys. J. R. astr. Soc.*, 74, 199-221.
- Chapman, S. and J. Bartels 1940. *Geomagnetism* (Oxford University Press, Oxford) p. 101.

Fung, S. F. 1996. Recent Developments in the NASA Trapped Radiation Models, pp. 79-91, in *Radiation Belts: Models and standards*, Ed. By J. F. Lemaire, D. Heynderickx, and D. N. Baker, AGU Geophysical Monograph 97.

Frasier-Smith, A.C., 1987, Centered and Eccentric Geomagnetic Dipoles and their Poles, 1600 – 1985.5, *Rev. Geophy.*, vol. 25, no. 1, 1 – 16.

Golightly, M.J., K. Hardy, and W. Quam 1994. Radiation dosimetry during U.S. Space Shuttle missions with the RME-III, *Radiat. Meas.*, 23, 25-42.

Heirtzler, J. R., 1999, *The Geomagnetic Field and Radiation in Near-Earth Orbits*, NASA/TM_1999_209481, 36 p.

Heynderickx, D., 1996, Comparison Between methods to Compensate for the Secular Motion of the South Atlantic Anomaly, *Radiation Measurements*, vol. 26, no. 3, 369-373.

Konradi, A., G.D. Badhwar, and L.A. Braby 1994. Recent space shuttle observations of the South Atlantic Anomaly and radiation belt models, *Adv. Space Res.*, 14(10), 911-921.

Laurients, M., A.L. Vampola, P. Inamti, and D. Bilitza 1995. Experimental validation of particle drift theories, paper presented at 32nd Informational Space Radiation Effects Conference, Int. of Electr. and Electron. Eng., Madison, Wis., July 17-21.

Pinto, O. Jr., and W. D. Gonzalez, 1989, SAMA: For how long?, *EOS Trans. AGU*, 70(2), 12.

Sabaka, T.J., R.A. Langel, R. T. Baldwin, and J. A. Conrad 1997. The Geomagnetic Field 1900-1995, Including the Large-Scale field from Magnetospheric Sources and the NASA Candidate Models for the 1995 Revision of the IGRF, *J. Geomag. Geoelectr.* 49, 157-206.

Figure Captions

Figure 1. Geomagnetic total field intensity, in nT, for 1995.0 based on IGRF 95. Contour interval 4000 nT.

Figure 2. Geomagnetic field lines leaving 20 S, 40 S, and 60 S for longitudes 40 W (left side) and 140 E (right side).

Figure 3. Height of geomagnetic field lines starting at 40 S, 30 S, and 20 S. The mirror points for particles with various equatorial pitch angles are marked, with the value of the equatorial pitch angle shown next to the point. These lines are along 60 W longitude and for the year 1995.0.

Figure 4. Places where Sudden Event Upsets occurred for the Topex/Poseidon spacecraft for the years 1992-1998. Contours of the geomagnetic total field intensity are shown for the altitude of the spacecraft (1340 km).

Figure 5. Dose rates for Mir and for Skylab as a function of latitude and of longitude. Mir's results were adjusted to Skylab's to compensate for altitude difference. (after Badhwar, 1997).

Figure 6. Secular variation of the total geomagnetic field intensity calculated from IGRF 95 coefficients (in nT/yr). Contour interval 20 nT/yr with negative values shown by dashed lines.

Figure 7. The change in the annual means of geomagnetic total field intensity for five geomagnetic observatories around the South Atlantic. Plots are shown for Vassouras, Brazil (VSS), Pilar, Argentina (PIL), Trelew, Argentina (TRW), Tsumba, Namibia (TSU), and Herman, South Africa (HER). The location of these observatories is shown in the panel at the upper left. Dotted lines, with accompanying numbers, show the least squares fit to a straight line for each observatory.

Figure 8. Geomagnetic total field intensity (in nT) for the year 2100, extrapolated from the year 1995.0 and using the IGRF 95 secular change coefficients. Contour interval 5000 nT.

Figure 9. Three geomagnetic field lines versus height for lines starting at 50 S, 40 S, and 30 S, along the Greenwich Meridian for the year 2100. Points along lines show where particles with a given pitch angle will mirror. The value of the equatorial pitch angle is shown next to the mirror position.

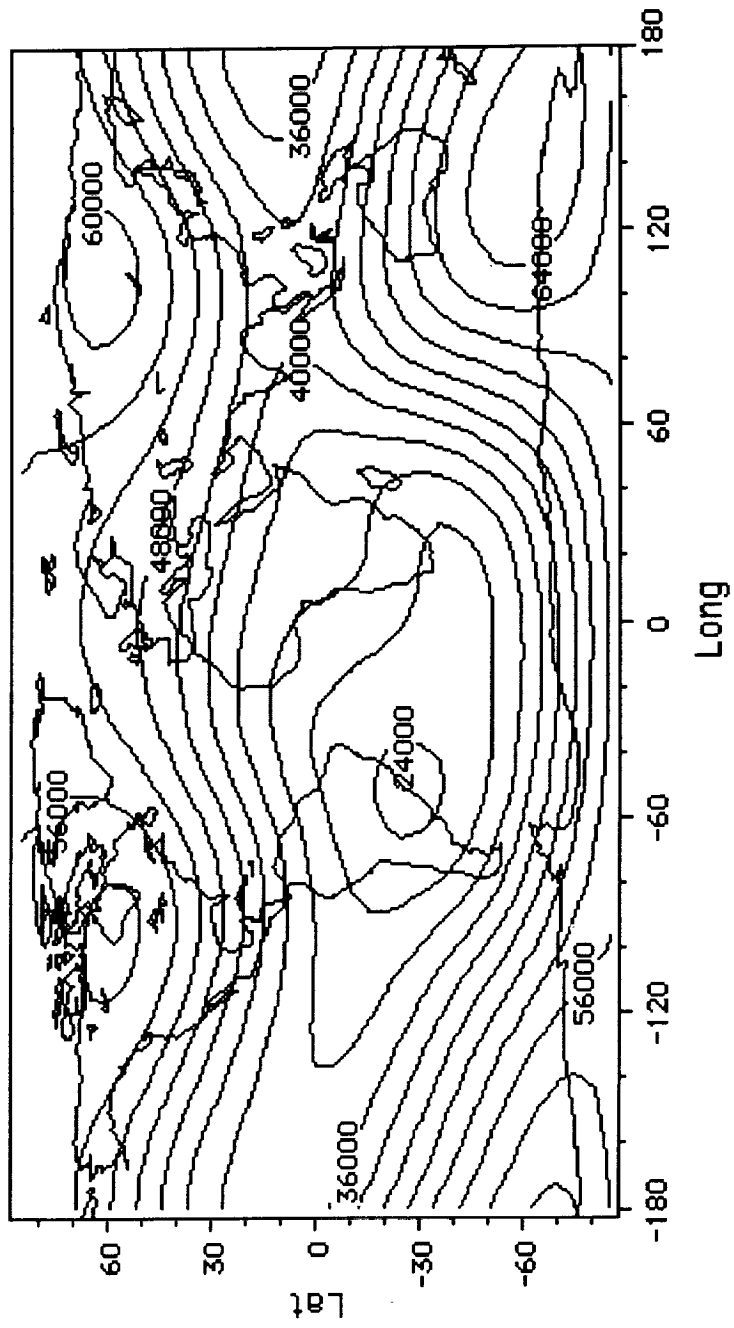


Fig 1

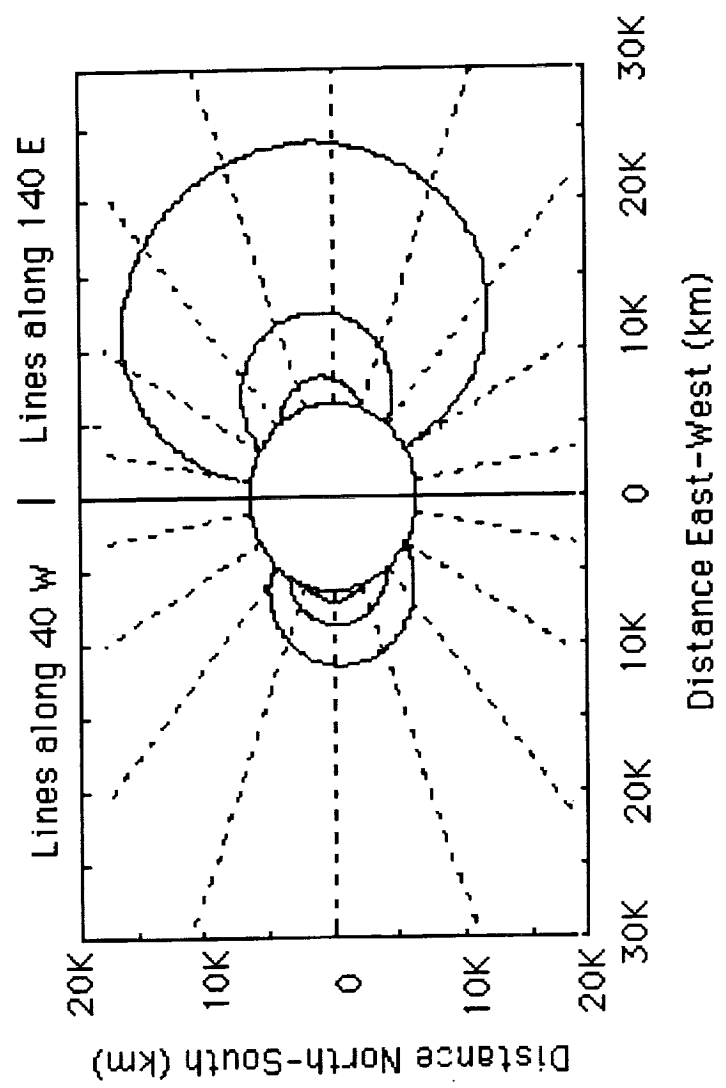


Fig. 2

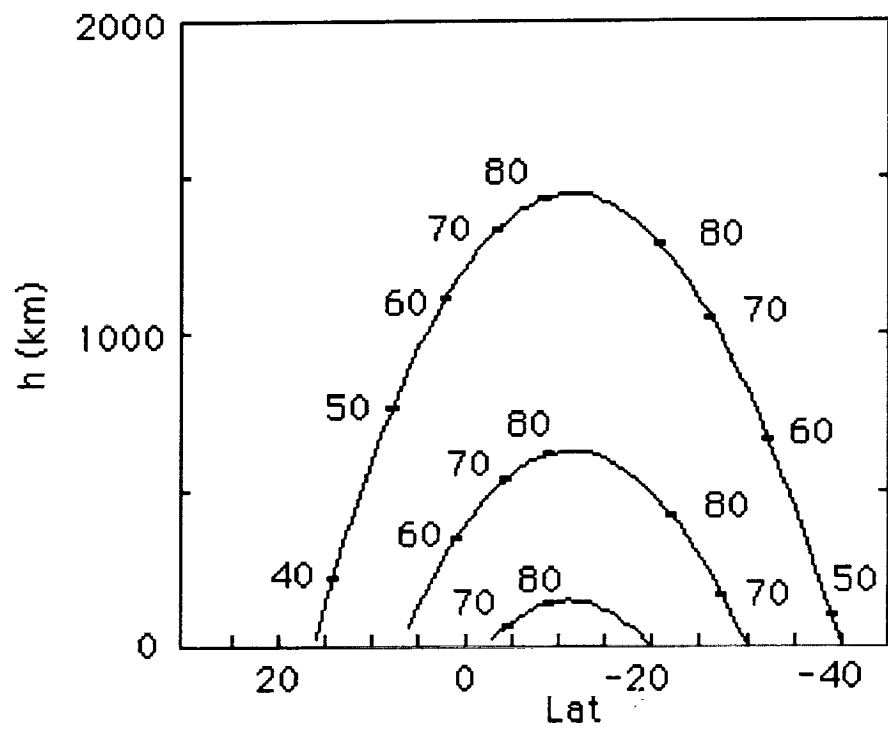


Fig. 3

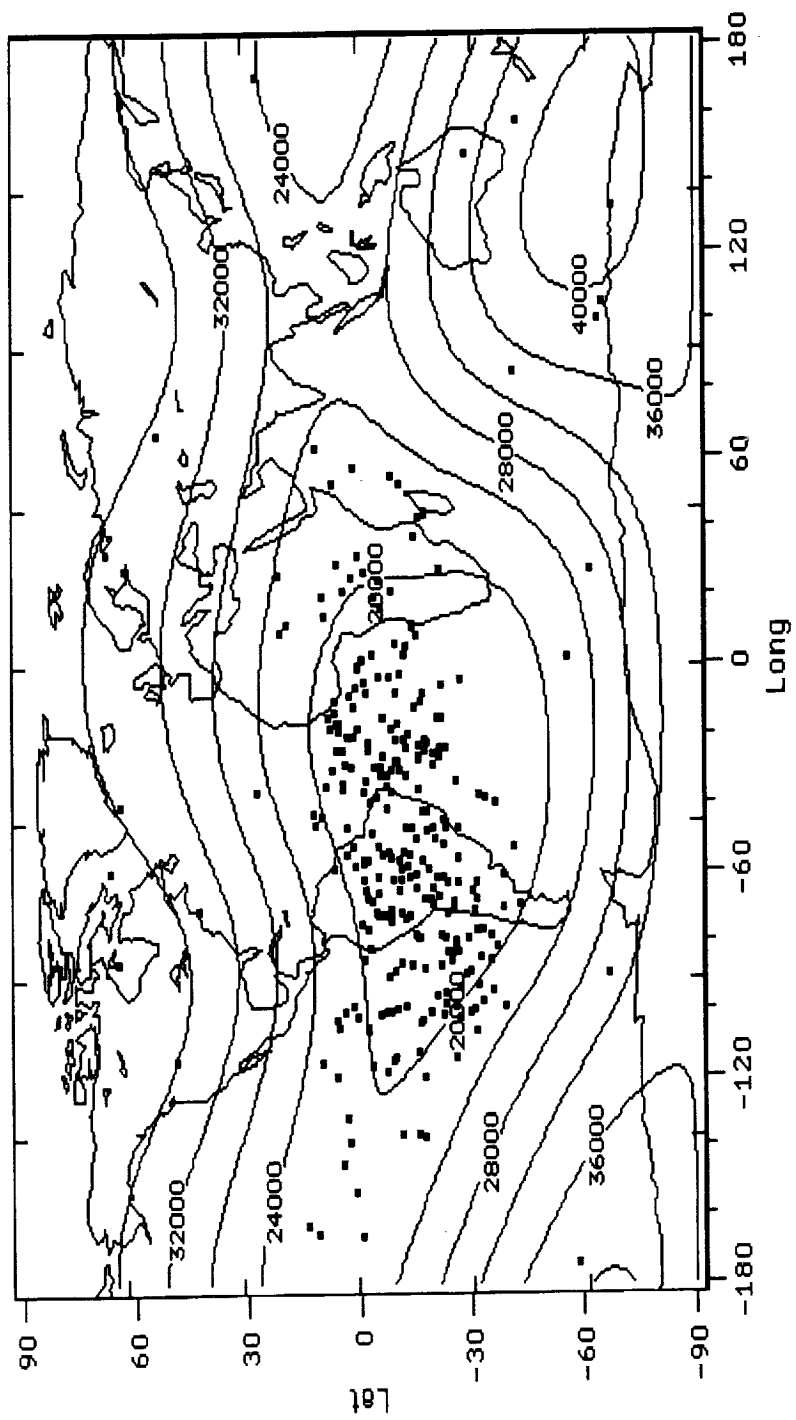
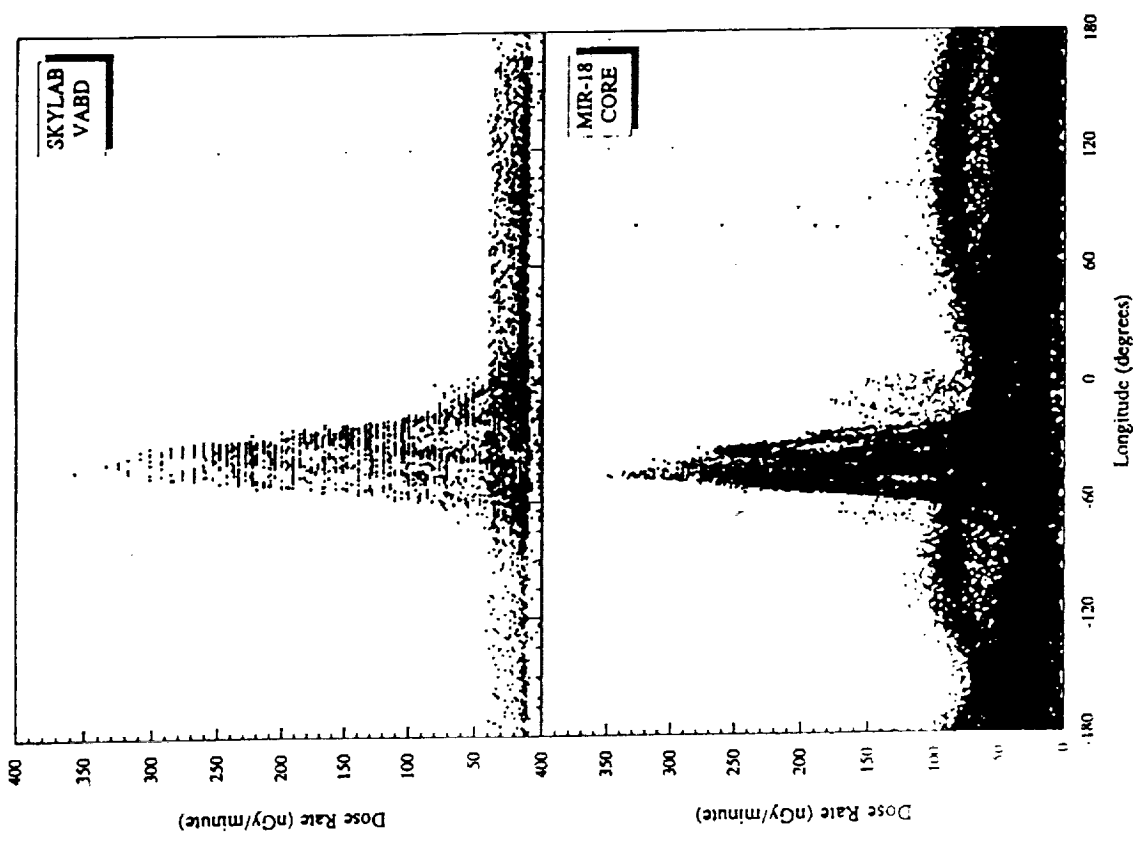
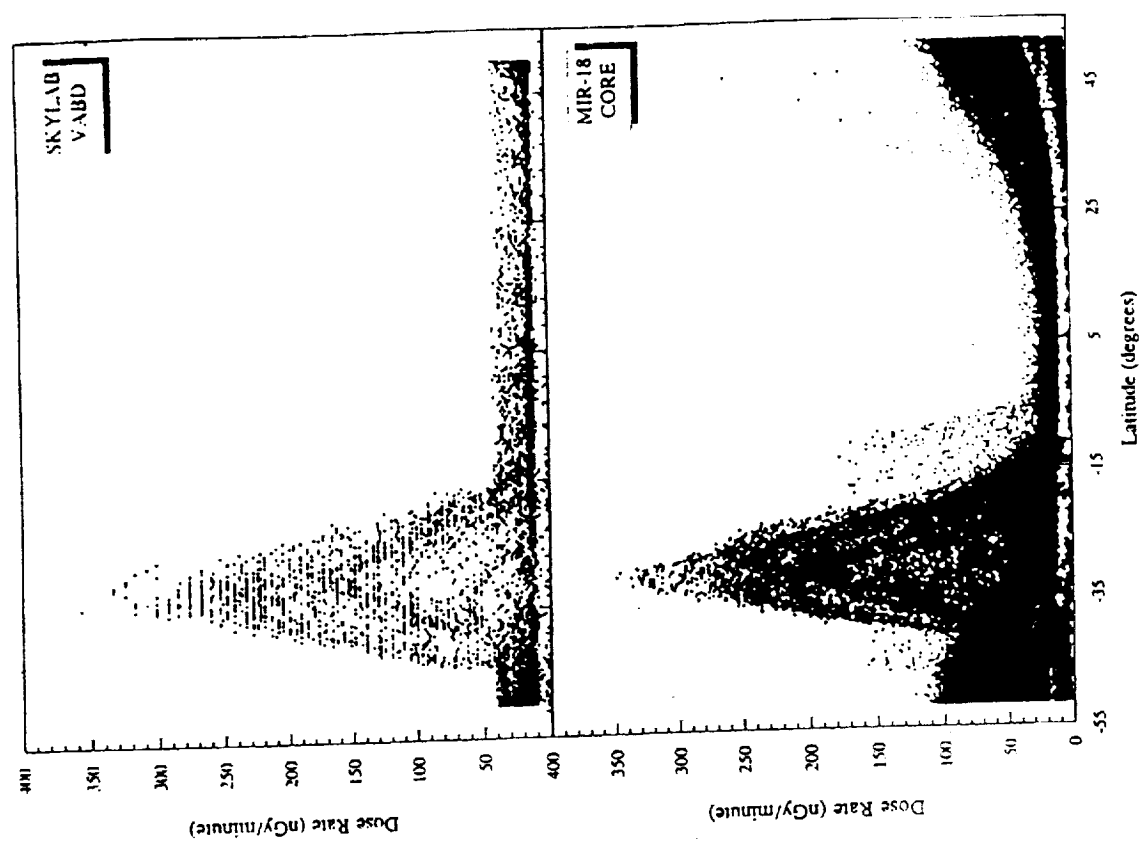


Fig. 4

Fig. 5



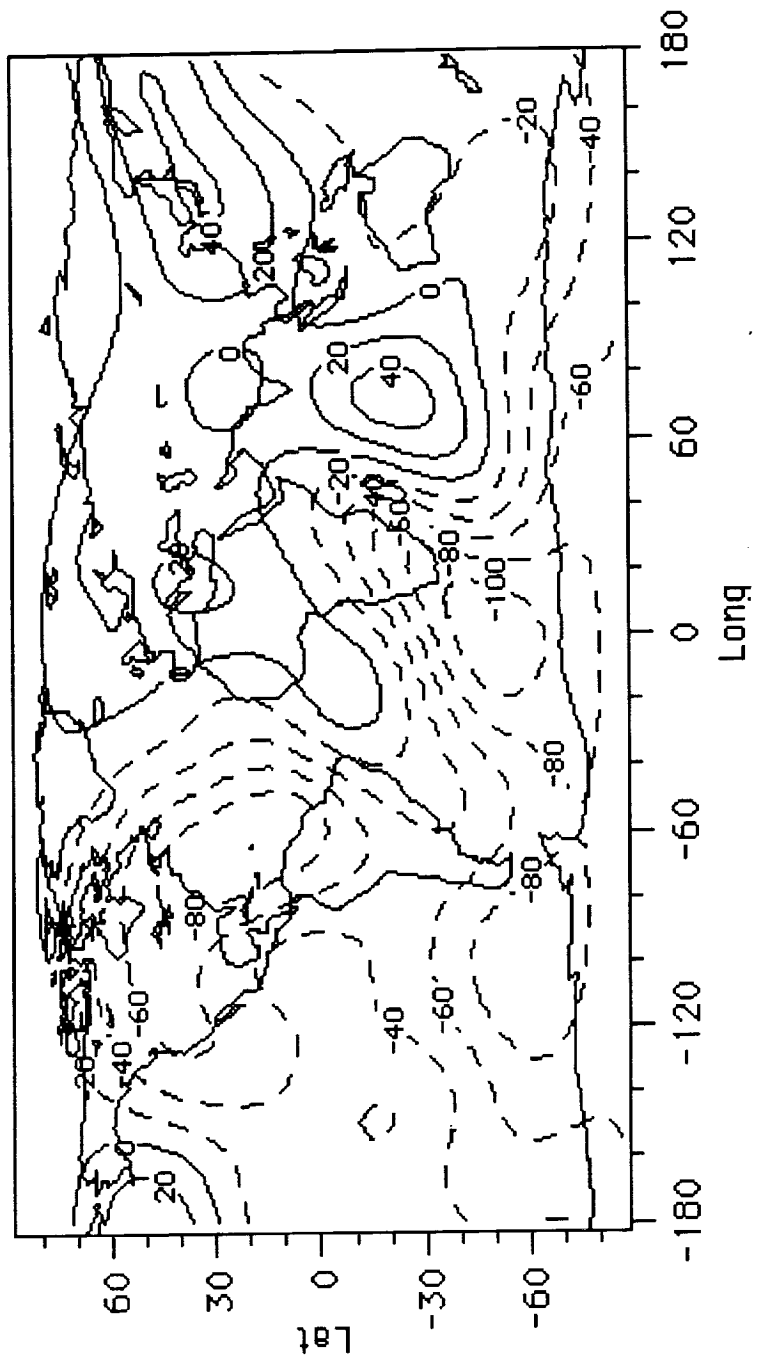


Fig. 6

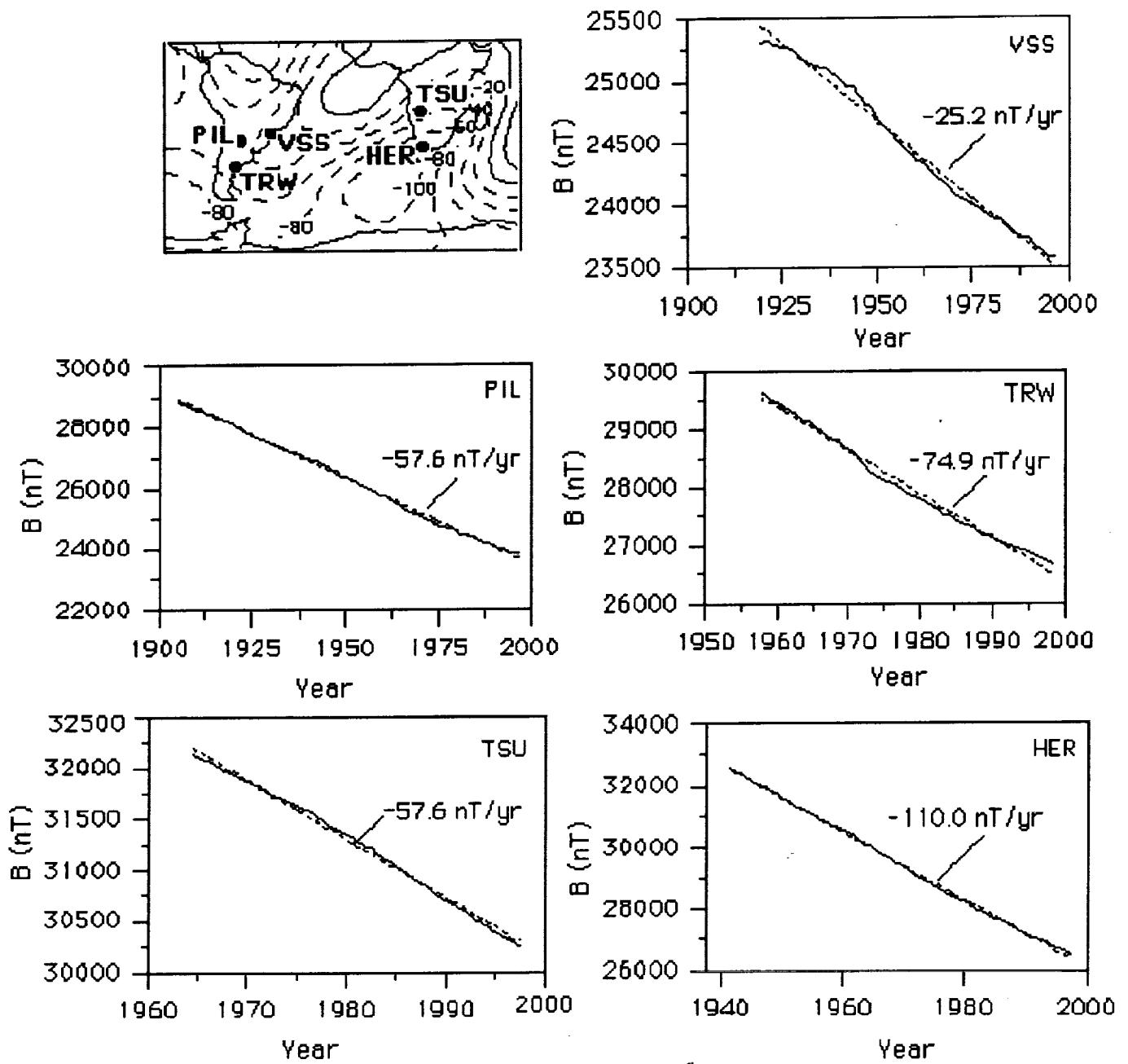


Fig. 7

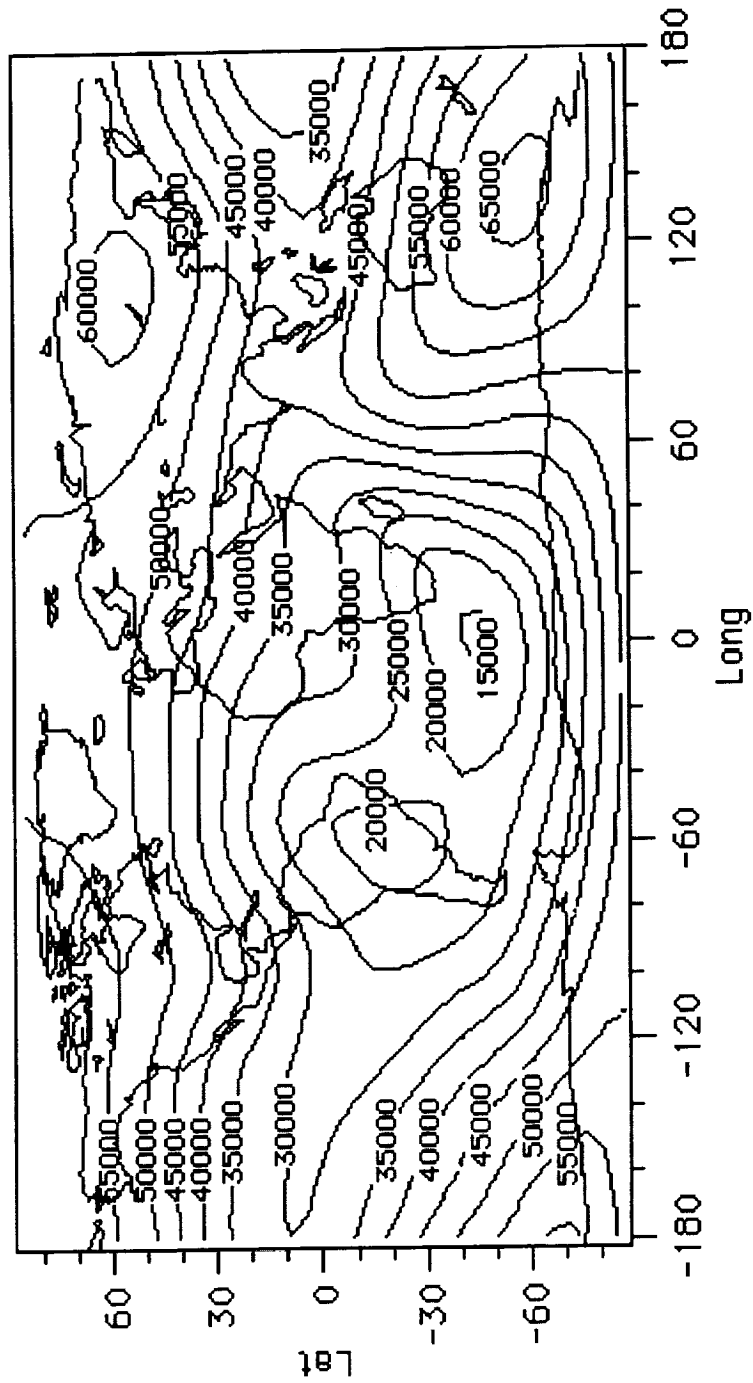


Fig. 8

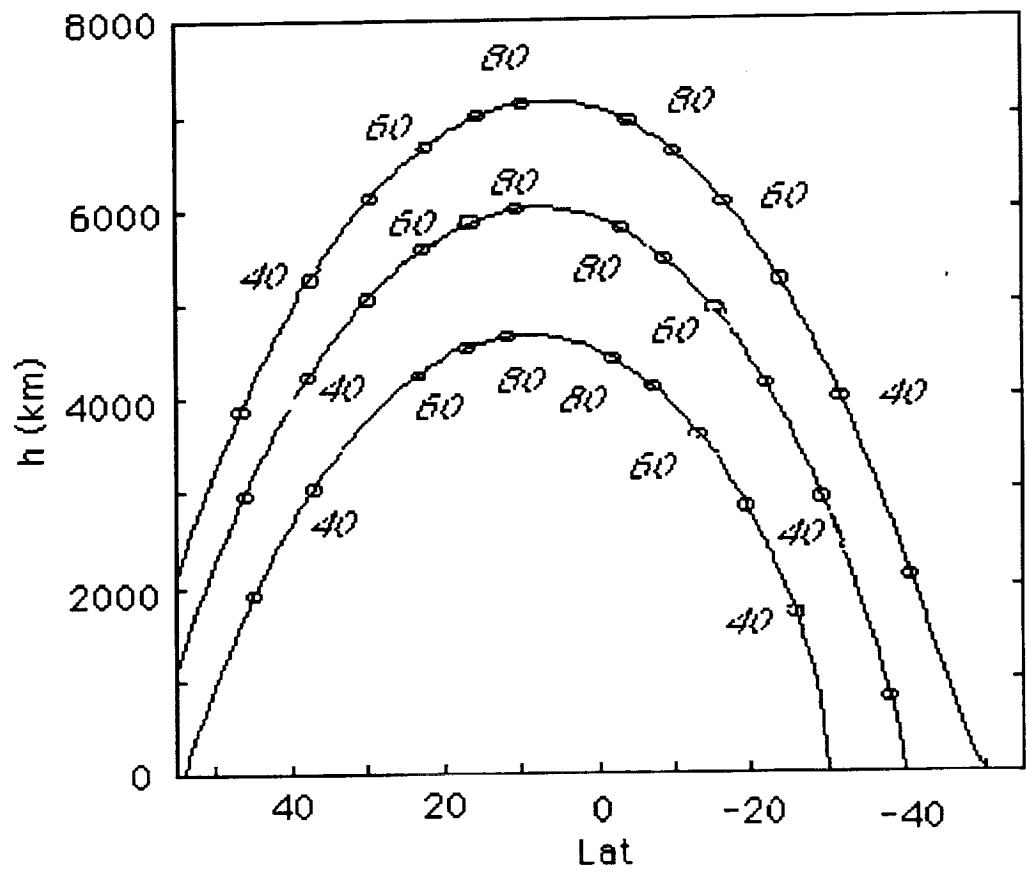


Fig. 9